JCB Article

MAP2 and tau bind longitudinally along the outer ridges of microtubule protofilaments

Jawdat Al-Bassam,[1] Rachel S. Ozer,[1] Daniel Safer,[2] Shelley Halpain,[1] and Ronald A. Milligan[1]

[1]Department of Cell Biology, Scripps Research Institute, La Jolla, CA 92037
[2]Department of Physiology, School of Medicine, University of Pennsylvania, Philadelphia, PA 19104

MAP2 and tau exhibit microtubule-stabilizing activities that are implicated in the development and maintenance of neuronal axons and dendrites. The proteins share a homologous COOH-terminal domain, composed of three or four microtubule binding repeats separated by inter-repeats (IRs). To investigate how MAP2 and tau stabilize microtubules, we calculated 3D maps of microtubules fully decorated with MAP2c or tau using cryo-EM and helical image analysis. Comparing these maps with an undecorated microtubule map revealed additional densities along protofilament ridges on the microtubule exterior, indicating that MAP2c and tau form an ordered structure when they bind microtubules. Localization of undecagold attached to the second IR of MAP2c showed that IRs also lie along the ridges, not between protofilaments. The densities attributable to the microtubule-associated proteins lie in close proximity to helices 11 and 12 and the COOH terminus of tubulin. Our data further suggest that the evolutionarily maintained differences observed in the repeat domain may be important for the specific targeting of different repeats to either α or β tubulin. These results provide strong evidence suggesting that MAP2c and tau stabilize microtubules by binding along individual protofilaments, possibly by bridging the tubulin interfaces.

Introduction

The microtubule cytoskeleton plays a fundamental role in a variety of cellular processes. Microtubules assemble by lateral association of protofilaments generated from head to tail polymerization of αβ tubulin dimers. The tendency of tubulin to switch stochastically between polymerization and depolymerization phases, termed dynamic instability (Mitchison and Kirschner, 1984), facilitates remodeling of the microtubule cytoskeleton for its various roles. Microtubule-associated proteins (MAPs)* influence dynamic instability by binding and stabilizing microtubules (Cleveland et al., 1977). The MAP2/tau family is a unique class of structural MAPs that modulate microtubule dynamics in neurons during the development of dendrites and axons (for reviews see Drewes et al., 1998; Goldstein and Gunawardena, 2000). Phosphorylation of MAP2/tau proteins at specific sites induces dissociation from microtubules (Drewes et al., 1997; Ozer and Halpain, 2000). However, hyperphosphorylation and/or specific mutations can promote aggregation of the dissociated tau into paired helical filaments, which are a hallmark of certain neurodegenerative diseases such as familial tauopathies and Alzheimer's disease (Crowther and Goedert, 2000; Garcia and Cleveland, 2001).

MAP2/tau proteins have dissimilar NH_2-terminal "projection" domains and homologous COOH-terminal microtubule binding domains. Studies investigating the cytoskeleton of neuronal processes showed that microtubules with MAP2 or tau bound are organized in parallel arrays in which the spacing between microtubules correlates with the length of the projection domains of the MAP (Hirokawa, 1982; Chen et al., 1992). Rotary shadowing experiments and circular dichroism studies on isolated MAP2/tau proteins indicate that they are highly extended polypeptides with little or no detectable secondary structure (Voter and Erickson 1982; Schweers et al., 1994).

The MAP2/tau microtubule binding domain contains three or four 18-residue microtubule binding repeats (MTBRs) separated by 13–14-residue inter-repeats (IRs) (Lewis et al., 1988; Himmler et al., 1989). Neighboring MTBRs within a given MAP share moderate homology; however, sequence alignment shows that repeats at identical positions in different MAP2s and taus are highly conserved (Fig. 1 A). There is evidence that IRs as well as MTBRs con-

Address correspondence to Ronald A. Milligan, Department of Cell Biology, CB-227, Scripps Research Institute, 10550 North Torrey Pines Road, La Jolla, CA 92037. Tel.: (858) 784-9827. Fax: (858) 784-2749. E-mail: milligan@scripps.edu

*Abbreviations used in this paper: cf-MAP2c, cysteine-free MAP2c; cIR-MAP2c, cysteine-IR-MAP2c; H11, helix 11; H12, helix 12; IR, inter-repeat; MAP, microtubule-associated protein; MTBR, microtubule binding repeat.

Key words: MAP2; tau; structure; microtubule; cryo-EM

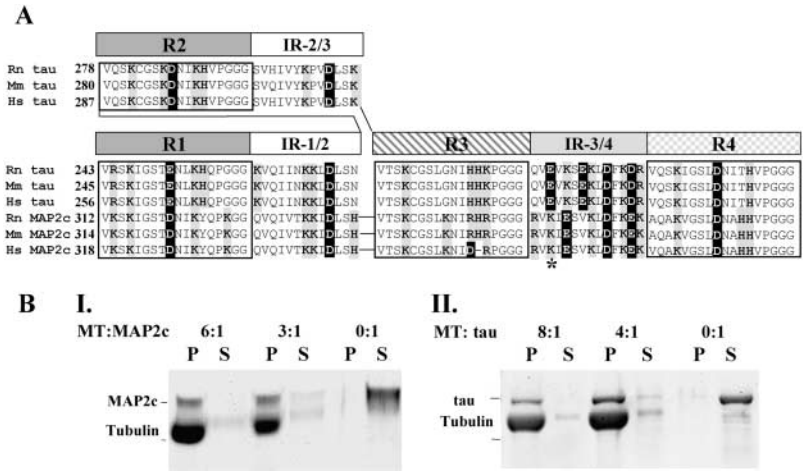

Figure 1. **Sequence homology and binding stoichiometry of MAP2c/tau.** (A) MTBRs and IRs of MAP2/tau have higher homology across species than with neighboring MTBRs and IRs. We performed MAP2/tau sequence alignment using Clustal W (Aiyar, 2000) with human (Hs), mouse (Mm), and rat (Rn) sequences of three-repeat MAP2c and four-repeat tau genes (GenBank/EMBL/DDBJ accession nos.: NP_114033 for Hs MAP2c; NP_005901 for Hs tau; AAA39490 for Mm MAP2c [extracted from MAP2b gene based upon consensus splice sites]; AAA58343 for Mm tau; CAA35667 for Rn MAP2c; NP_058908 for Rn tau). Above the aligned sequences, we show a schematic diagram of MTBRs (labeled R1–R4) and IRs. IRs are labeled according to the designation of the repeats that precede and follow them (e.g., the IR between repeats 3 and 4 is designated "IR-3/4"). Positively charged residues (shaded in gray) and negatively charged residues (shaded in black) are highly conserved at identical positions of the repeat domains. Based upon residue conservation, IR-3/4 modules are quite different from IR-1/2 or IR-2/3 modules. In four-repeat tau, alternative splicing introduces an additional MTBR-IR module (R2 and IR-2/3, upper left) that is very similar to R1 and IR-1/2 modules (for ease of sequence comparison, we depict the added module as shown, actual splice boundaries differ; see Goode and Feinstein, 1994, for details). The comparisons suggests that R2, IR-2/3 modules have higher homology to R1, IR-1/2 modules than to R3, IR-3/4 modules, respectively. The asterisk identifies Lys-364 in IR-3/4 where the undecagold was attached. (B) MAP2c and tau bind microtubules with different stoichiometries. MAP2c binding to microtubules is measured by cosedimentation with microtubules in the pellet (P) and depletion from the supernatant (S). In I, MAP2c does not sediment in the absence of microtubules (0:1). Each MAP2c binds 2.4 tubulin monomers. Saturation is indicated by MAP2c remaining in the supernatant (S lanes) at the 3:1 ratio compared with the 6:1 ratio. In II, cosedimentation assays indicate that tau saturates microtubules at one molecule of tau to 3.8 tubulin monomers. At the saturating ratio of tubulin to tau (4:1), the supernatant (S) contains unbound tau compared with the lower ratio (8:1) where all tau is bound to microtubules.

tribute to microtubule binding (Butner and Kirschner, 1991; Goode and Feinstein, 1994; Ludin et al., 1996). The affinity of the repeat domain for microtubules and its polymer stabilizing activity both increase with the number of MTBR-IR modules (Ludin et al., 1996; Goode et al., 2000). Binding to microtubules is mediated, in part, by the acidic tubulin COOH termini (Paschal et al., 1989), because their removal by subtilisin reduces MAP binding (Serrano et al., 1984, 1985).

The prevailing model to explain how MAP2/tau family proteins interact with microtubules presumes that each MTBR-IR module interacts with a separate, but adjacent, tubulin monomer within the microtubule wall (Butner and Kirschner, 1991; Gustke et al., 1994). Despite considerable study, the structural basis for MAP2/tau stabilization of microtubules is not understood. It remains unclear whether increased microtubule stability is achieved by MAPs binding along protofilaments (a longitudinal binding model) or wrapping around the microtubule (a lateral binding model). As microtubule disassembly proceeds by protofilaments separating and curling outwards at the ends of the microtubule (Mandelkow et al., 1991), longitudinal binding could account for increased microtubule stability by strengthening tubulin interactions along protofilaments and preventing outward curling. Alternatively, in the lateral binding model, the wrapped MAPs would prevent protofilament separation (Ichihara et al., 2001).

Here we have used cryo-EM and helical image analysis to determine the geometry of MAP2c and tau binding to microtubules. We show that MAP2c- or tau-decorated microtubules have additional ordered density along protofilament ridges compared with undecorated microtubules. We used undecagold labeling to show that the IRs lie along the ridges and not between protofilaments. The gold labeling data suggest that the MTBR-IR modules may be uniquely targeted to α or β tubulin. Taken together, our results suggest that MAP2 and tau proteins reduce microtubule depolymerization by bridging and stabilizing the tubulin–tubulin interfaces along protofilaments.

Results

Cryo-EM of MAP2c- and tau-decorated microtubules

To investigate how MAPs stabilize microtubules, we have analyzed two distinct proteins using cryo-EM and helical image analysis: a recombinant three-repeat rat MAP2c (termed MAP2c throughout) and a recombinant four-repeat human tau (termed tau throughout). The MAP2c and tau proteins are homologous in their repeat domain, but tau includes an additional MTBR-IR module (Fig. 1 A; see Materials and methods).

We used cosedimentation assays to determine conditions for full decoration of microtubules by MAP2c and tau. Under saturating conditions, MAP2c bound microtubules at a ratio of one molecule for every 2.4 tubulin monomers (Fig. 1 B, I), and tau at one molecule for every 3.8 tubulin monomers (Fig. 1 B, II). These stoichiometry values are very similar to those determined by others (Gustke et al., 1994; Coffey and Purich, 1995). We used the conditions found for maximal binding to prepare decorated microtubules for cryo-EM.

Images of microtubules decorated with either MAP2c or tau were visually indistinguishable from those of undecorated microtubules (Fig. 2 A). Both the diameter and moiré (super-twist) repeat length of decorated 15-protofilament helical microtubules were similar to those of undecorated microtubules (Fig. 2 B), indicating that binding of MAP2c or tau does not induce large changes in the microtubule

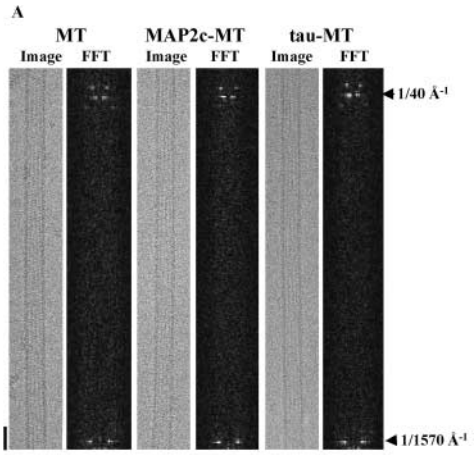

B

Data Sets	Repeats	Asymmetric units	Diameter	Moiré length
MTs	285	~41000	220±2.4	1501±41
MAP2c-MTs	194	~27900	221±3.1	1589±84
tau-MTs	129	~18500	223±3.3	1602±103

Figure 2. **The binding of MAPs to microtubules does not induce changes to their architecture.** (A) Images and power spectra (FFT) of MAP2c-decorated microtubules (MAP2c-MT), tau-decorated microtubules (tau-MT), and undecorated microtubules (MT) are visually indistinguishable. Only one half of each power spectrum (FFT) is shown and it is compressed 16-fold in the equatorial direction. Bar, 300 Å. (B) Number of moiré repeats and asymmetric units contributing to the final data are listed together with average microtubule diameter and average moiré length (in angstroms) for each dataset.

structure. Although individual images of decorated and undecorated microtubules look similar, differences were evident after averaging the layer line data from a number of images. In particular, layer line 1 amplitudes were stronger for decorated microtubules (Fig. S1, available at http://www.jcb.org/cgi/content/full/jcb.200201048/DC1) with minor changes in other layer lines, consistent with an increase in protofilament density. There were no additional layer lines in the decorated microtubules, as would be expected if the MAP projection domains were contributing to off-equatorial diffraction (Amos, 1977).

MAP2 and tau are ordered on microtubule protofilaments

From the averaged layer lines, we calculated 3D maps of MAP2c-decorated, tau-decorated, and undecorated microtubules. All three maps show the same general features as those previously reported for microtubules (Sosa et al., 1997; Nogales et al., 1999). However, consistent with the differences in the layer lines, there is additional density lying along the protofilament ridges of the decorated microtubule maps (Fig. S2). To more clearly visualize this density, which is presumably attributable to MAP2c or tau binding, we performed difference mapping (Fig. 3) and statistical analyses (Fig. S3).

The difference maps, which were statistically significant at the $P = 0.0001$ level, show elongated density along the protofilament ridges on the outside of the microtubule (Fig. 3, C–F, and Fig. S3, A–D). The MAP2c and tau difference densities, between which there were no statistically significant differences (unpublished data), have a slender cross section compared with tubulin (Fig. 3, D and F). Although the difference densities are continuous along the surface of the protofilament, there are variations suggesting two density peaks associated with each tubulin monomer (Fig. 3, C and E). There are subtle differences in the density peaks associated with adjacent monomers, but it is not clear if they are meaningful.

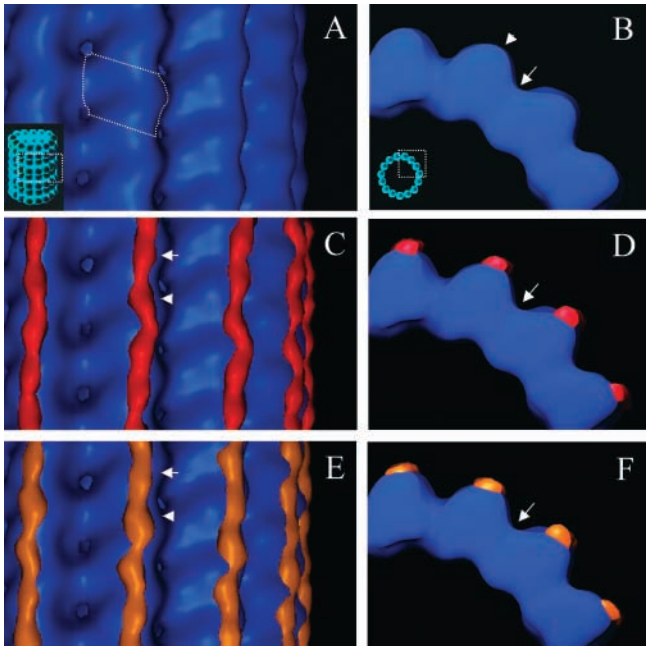

Figure 3. **MAP2c and tau form ordered densities protofilament ridges.** (A) En face view of the undecorated microtubule map showing four protofilaments. A tubulin monomer is outlined by a dotted line. (B) View of the undecorated microtubule map from the minus end showing the smooth curvature of protofilament ridges (arrowhead) separated by valleys between protofilaments (arrow). (C and E) En face views of MAP2c (red) and tau (orange) difference maps displayed with the microtubule map (blue). Arrows and arrowheads indicate two different density peaks in the elongated difference map associated with each 40-Å longitudinal repeat of tubulin. (D and F) Views of C and E from the microtubule minus end showing the slender profile of MAP2c and tau densities compared with tubulin. No difference densities are seen in the valleys between protofilaments (arrows).

The COOH termini of α and β tubulin are disordered in undecorated microtubules (Nogales et al., 1998), but are directly involved in MAP2 and tau binding. Therefore, we interpret the elongated difference maps to represent the MAP2 and tau repeat domains together with the tubulin COOH termini. Even though we did not observe any difference density in the valleys between protofilaments (Fig. 3, D and F, arrows), these difference maps still allow for the possibility that the MAP2c and tau proteins bind laterally across protofilaments; the 13–14-residue IR could stretch between adjacent protofilaments but would not be visualized at the resolution of this study.

MAP2/tau proteins bind longitudinally along protofilaments

To distinguish between lateral and longitudinal binding geometries, we used undecagold labeling to locate IR-3/4 of MAP2c. The single natural cysteine (Cys 348) present in MAP2c was first replaced by a serine, thereby generating a cysteine-free MAP2c (cf-MAP2c). This mutant protein

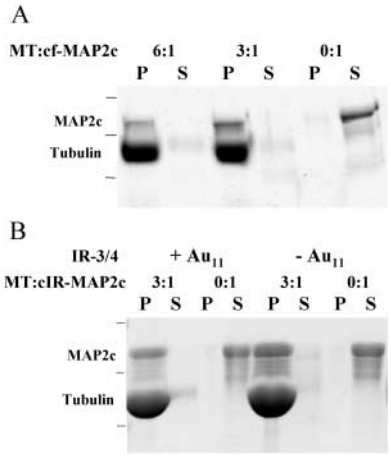

Figure 4. **Neither Cys mutagenesis nor Au_{11}–IR-3/4 labeling of MAP2c interfere with overall microtubule binding.** (A) Examples of cosedimentation analysis of cf-MAP2c and microtubules. Each cf-MAP2c binds 2.8 tubulin monomers at saturation, and it only pellets in the presence of microtubules. Supernatants (S) and pellets (P) at molar ratios of 0:1, 3:1, or 6:1 (tubulin/MAP2c) are shown. (B) Each unlabeled cIR-MAP2c ($-Au_{11}$) bound 2.6 tubulin monomers and each gold-labeled cIR-MAP2c ($+Au_{11}$) bound 2.5 tubulin monomers.

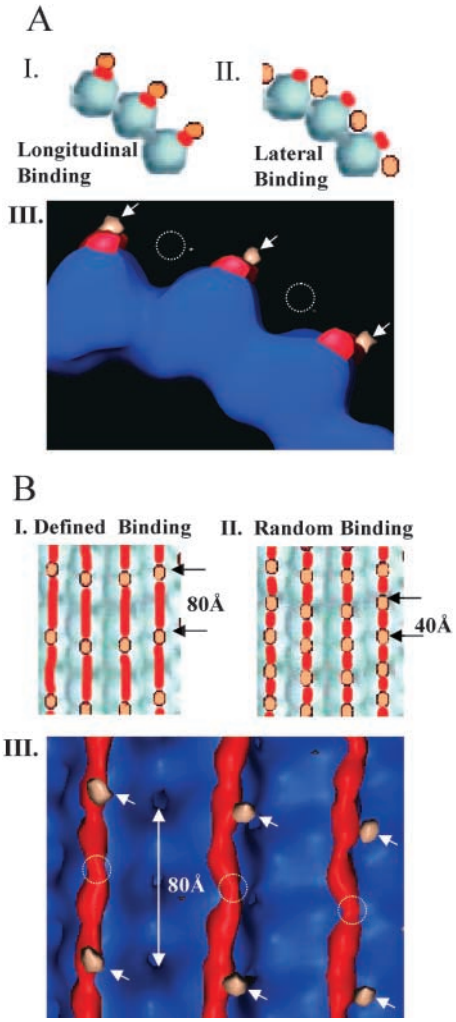

Figure 5. **Longitudinal binding of MAP2c along protofilaments.** (A) MAP2c binds longitudinally along single protofilaments and not laterally across multiple protofilaments. The two possible models would result in different localizations of Au_{11} attached to IR-3/4. In I, the longitudinal binding model would result in the Au_{11} lying on top of the protofilament ridges. In II, the lateral binding model would lead to Au_{11} lying in the valleys between protofilaments. In III, a view from the minus end shows that the Au_{11} difference map (tan) is only present on top of the MAP2c difference densities (red). This result supports the longitudinal binding model (arrows) and excludes the lateral binding model (broken circles). (B) Averaging during image analysis leads to outcomes that suggest specific targeting to α or β tubulin. If specific targeting occurs, the Au_{11} attached to IR-3/4 will only be visualized when the data is averaged assuming an 80-Å tubulin repeat (I). With nonspecific (i.e., random) binding of MAP2c repeats, averaging assuming either 40- or 80-Å repeats will result in visualization of the Au_{11} every 40 Å (II). Both specific and random binding modes occur at the same saturation stoichiometry. In III, an en face view of A III is shown. The difference peaks attributable to Au_{11} (tan, arrows) were only visualized when the data were averaged taking into account 80-Å tubulin heterodimer periodicity. This result suggests specific targeting of the MTBR-IRs to either to α or β tubulin. Dotted circles signify the absence of difference peaks that would be expected if random binding occurred.

bound microtubules with the same stoichiometry as MAP2c (Fig. 4 A). We then introduced a cysteine in place of lysine 364 (Fig. 1 A, asterisk) in IR-3/4 of cf-MAP2c generating a cysteine-IR-MAP2c mutant (cIR-MAP2c), which we conjugated to undecagold (Au_{11}) (Milligan et al., 1990; Safer, 1999; Rice et al., 1999). We confirmed that neither the mutation nor Au_{11} attachment interferes with cIR-MAP2c binding to microtubules (Fig. 4 B). The 3D map calculated from Au_{11}–cIR-MAP2c–decorated microtubules showed an additional knob-like density on the microtubule surface. Difference mapping and statistical analysis showed that this density was statistically significant at the $P = 0.001$ level (Fig. 5 and Fig. S3, E and F).

These experiments allow us to distinguish between the longitudinal and the lateral binding models by localization of the undecagold and by inference the IR-3/4 to which it is attached. The two possible positions of the IR–Au_{11} would either be on the protofilament ridges, if MAP2c binds microtubules longitudinally (Fig. 5 A, I), or in the valleys between protofilaments, if it binds microtubules laterally (Fig. 5 A, II). The undecagold difference map clearly indicates that IR-3/4 lies on top of the MAP2c difference densities along the protofilament ridges (Fig. 5 A, III). Thus, the IRs lie between bound MTBRs along the ridges (Fig. 5 A, III, arrows), consistent with a longitudinal binding model.

The repeat domain recognizes α and β tubulins uniquely

Unexpectedly, we observed an additional degree of specificity in the Au_{11}–IR-3/4 localization. As α and β tubulins are indistinguishable at the resolution of this study, either tubulin monomer (40-Å repeat) or dimer symmetry (80-Å repeat) may be imposed during averaging. With longitudinal binding and nonspecific MTBR-IR module attachment to α or β tubulins, image analysis and averaging would yield an undecagold difference peak at every tubulin monomer irrespective of whether monomer or dimer symmetry is applied (Fig. 5 B, II). On the other hand, if MTBR-IR modules uniquely target α or β tubulin, the undecagold difference peak will only be visualized when dimer symmetry is imposed (Fig. 5

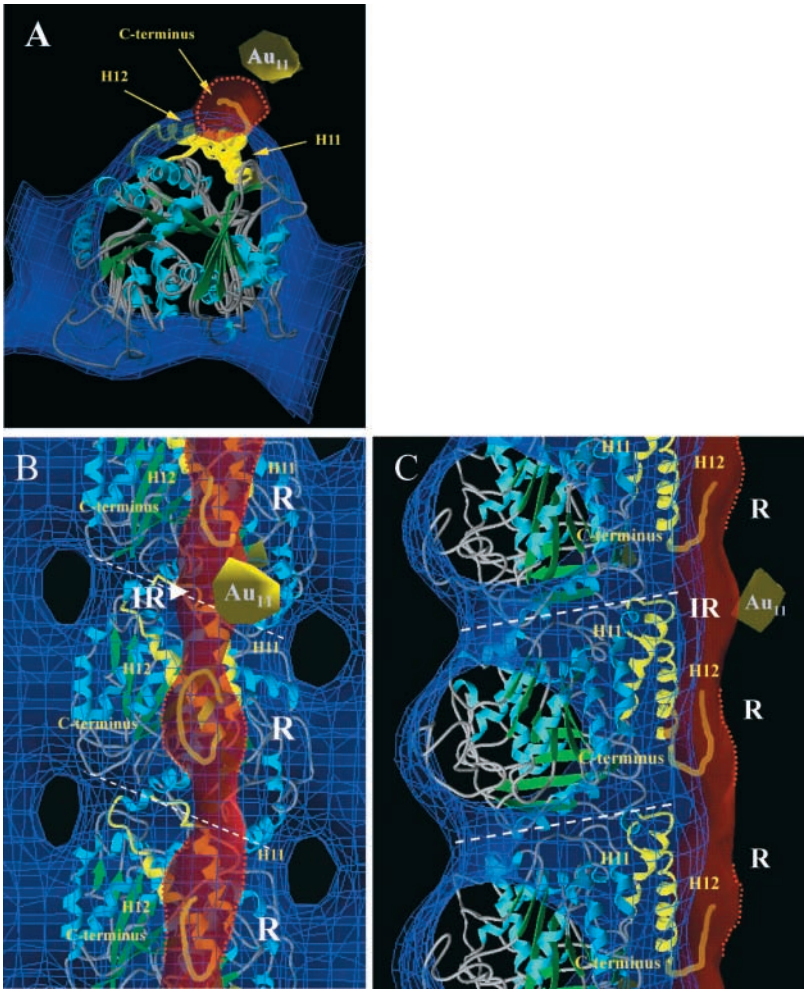

Figure 6. **MAP2c lies over H11, H12, and COOH termini of tubulin along the protofilament ridges.** (A) View from the minus end of the protofilament structure (Protein Data Bank identification no. 1TUB) docked into the microtubule map (blue wire frame). Tubulin H11 and H12 (yellow) are on the external protofilament ridges and appear to be the primary binding sites for the MAP2c difference map (enclosed by dotted red lines). The tubulin COOH termini (orange, modeled in arbitrary conformations) extend into the MAP2c difference map. Other helices and sheets in the tubulin structure are blue and green, respectively. (B and C) En face and side views (respectively) showing that the undecagold difference map (Au_{11}) and, hence, IR-3/4 lie close to the tubulin–tubulin interface (dashed white lines) and are associated with one of the high-density peaks in the MAP2c difference map (red). The IR lies over the COOH-terminal part of H11. The second density peak of the MAP2c difference map lies over the end of H12 and the exit site of the tubulin COOH terminus. It is attributable to the MTBR and the tubulin COOH terminus (red dotted lines).

B, I). We analyzed our data imposing either monomer or dimer symmetry and were only able to visualize the undecagold when we used dimer symmetry (Fig. 5 B, III). These data strongly argue in favor of specific binding of IR-3/4 to either α or β tubulin, but not to both (Fig. 5 B, III).

The repeat domains bind helix 11 (H11), helix 12 (H12), and the COOH termini of tubulin

Although there is considerable evidence showing that MAP2 and tau are unstructured in solution (Voter and Erickson, 1982; Schweers et al., 1994), the data presented here show that they form ordered densities along the protofilament ridges when they bind microtubules. Thus, it seems likely that specific residues on the protofilament surface are required to fold the MTBR-IR modules and induce the bound density that we observe. To investigate which structural elements on the tubulin surface are likely to induce the IRs and MTBRs to fold, we manually docked the atomic coordinates of the αβ tubulin dimer into the microtubule map and displayed the result with the MAP2c and undecagold difference maps. As the tubulin COOH termini (18 and 10 residues for α and β tubulins, respectively) are disordered and not resolved in the structure (Nogales et al., 1998), we modeled these parts of the molecule to show where they exit the protofilament surface (Fig. 6 A). MAP2c difference densities are closely apposed to helices 11 (H11) and 12 (H12), which are the prominent structural elements of tubulin exposed on the outer surface of microtubules. The last resolved residues of the tubulin COOH terminus are positioned directly below the MAP2c difference map (Fig. 6 A).

The undecagold difference map lies directly over the tubulin–tubulin interface close to the COOH-terminal end of H11 (Fig. 6, B and C). This implies that the IR, to which the undecagold is attached (Fig. 1 A, asterisk), also binds to the interface, the region of the structure that has been shown to directly modulate the protofilament conformation in growth and catastrophe (Mandelkow et al., 1991; Nogales et al., 1999; Gigant et al., 2000). In light of this localization of the IR, the MTBR portion must lie centrally on the tubulin monomer in close proximity to the end of H12 and the exit site of the tubulin COOH terminus (Fig. 6, B and C). This position coincides with an increase in density along the length of the MAP2c difference map, which may be attributable to an ordered domain containing the tubulin COOH terminus and the MTBR (Fig. 6 B). The effects of MAP binding on these tubulin elements may translate into the microtubule-stabilizing activities of the MAP2c/tau proteins.

Discussion

The binding of each 31–32-residue MTBR-IR module of the MAPs to a single tubulin monomer is supported by our data on the stoichiometry of binding as well as peptide and

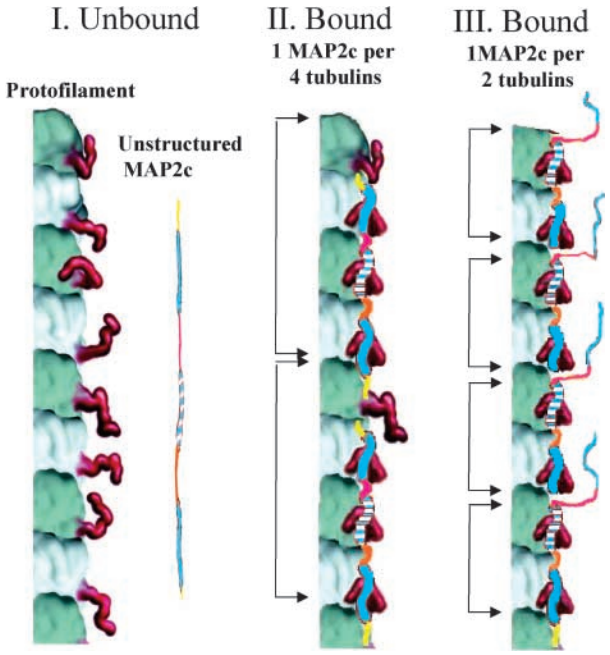

Figure 7. **Model for MAP2c repeat domain binding to protofilaments.** The MAP2c repeat domain (three repeats shown as an ~280-Å-long strand) and the tubulin COOH termini (red, in arbitrary conformation) are unstructured as shown in I (the protofilament illustration is reproduced from *The Journal of Cell Biology*, 2000; 151, 1093–1110 by copyright permission of the Rockefeller University Press). During binding, the MAP2c repeat domain interacts with the tubulin COOH termini, becomes compacted, and localizes on the outer surface of the protofilament. A combination of two binding geometries (II and III) is required to explain both the observed binding stoichiometry and the gold labeling data showing specific targeting of repeats to either α or β tubulin. In II, all three repeats of MAP2c are specifically bound to a protofilament and there are gaps (one unbound tubulin monomer) between adjacent MAP2c molecules. In III, only two of the MAP2c repeats are bound and there are no gaps along the protofilament. The central repeat of MAP2c (blue stripes) has the highest affinity (Coffey et al., 1994; Ludin et al., 1996). In both binding geometries, the repeat domain has a specific orientation with respect to the tubulin dimer and the IRs bridge the tubulin interfaces. The MAP2c projection domain is not represented here, and the polarity of the repeat domain is not known.

deletion studies by others (Lee et al., 1989; Ludin et al., 1996). There is considerable evidence that MAPs are unstructured in solution (Voter and Erickson, 1982; Schweers et al., 1994) where, if fully extended, a module could be up to 110 Å long. Therefore, a module binds to the 40-Å-long tubulin monomer either in a loose, largely unstructured association or it must become ordered. There is some evidence from NMR studies for a disordered to ordered transition upon microtubule binding (Kotani et al., 1990). Our analysis reveals elongated, extended density on the outer surface of the protofilament when MAP2c or tau bind to microtubules. These structural data together with the stoichiometry results provide strong evidence for formation of an ordered association, as the image averaging procedures we used would not allow visualization of a loose unstructured association. It follows that the MTBR-IR module must undergo up to an approximately threefold reduction in length concomitant with the disordered to ordered transition when it interacts with the tubulin monomer (Fig. 7). There is precedent for such a large conformation change; folding upon binding has been observed in many protein–protein or protein–nucleic acid complexes and it has been suggested that flexibility of the components might lower the energy barrier for formation of a folded complex (for reviews see Williamson, 2000; Dyson and Wright, 2002).

At first glance, the binding stoichiometry of one three-repeat MAP2c molecule for approximately three tubulin monomers, shown here and by others (Coffey and Purich, 1995), seems inconsistent with the specific targeting observed in our undecagold labeling experiments. Specific targeting of MTBR-IR modules to either α or β tubulin would predict the occurrence of gaps between bound MAP2c molecules along the protofilament (Fig. 7 II), and lead to a binding stoichiometry of 1:4 for a MAP with three modules. However, more MAP2c can bind than is predicted by this model. One way to reconcile these findings is to suggest that there is variation in the binding geometry (Fig. 7). In this model, the observed stoichiometry is a consequence of there being two types of interaction: one in which all three MTBR-IR modules are attached and there are gaps between successive MAP molecules along the protofilament (Fig. 7 II), and one in which only two of the three MTBR-IR repeats are attached (Fig. 7 III). This model satisfies both the observed stoichiometry and our data on specific targeting.

MAP2 and tau may stabilize protofilaments by bridging tubulin interfaces

Our data support a previously proposed model that longitudinal binding of the MAP2/tau proteins to protofilaments leads to microtubule stabilization by bridging the tubulin interfaces (Dye et al., 1993). It is likely that the longitudinal MAP2/tau binding stabilizes a specific conformation of the tubulin interdimer interface. The conformation of this interface depends on the state of guanosine nucleotide in β tubulin. The GTP-bound state mediates straight interdimer interfaces and maintains straight protofilaments (Muller-Reichert et al., 1998). In the absence of the GTP cap, the GDP-bound state leads to curved protofilaments (Gigant et al., 2000), which promote microtubule catastrophe. By bridging tubulin–tubulin interfaces axially, we suggest that MAP2/tau binding along protofilaments may stabilize a straight GDP conformation and produce a cumulative effect along their length. Furthermore, longitudinal binding is consistent with evidence showing that the binding of MAP2c and tau decreases flexibility of microtubules (Dye et al., 1993; Felgner et al., 1997). In contrast, taxol-induced stabilization slightly increases microtubule flexibility (Mickey and Howard, 1995; Felgner et al., 1997). This distinction may underlie the observed differences between the action of taxol and MAP2/tau proteins in vivo (Spero and Roisen, 1985; Leclerc et al., 1996).

The effect of MAP2/tau on stabilizing straight protofilaments by longitudinal binding is consistent with their observed effects on microtubule dynamics. At low concentrations, MAP2/tau proteins decrease the frequency of catastrophes and dramatically increase the frequency of rescues (Joly et al., 1989; Kowalski and Williams, 1993; Gam-

blin et al., 1996). Furthermore, rescues tend to occur at regions in microtubules where MAP2 and tau proteins are bound, suggesting that the protofilaments are less likely to curl at such regions (Ichihara et al., 2001). Below the critical concentrations of tubulin, MAP2/tau proteins inhibit microtubule catastrophes and lead to "stalled" microtubule ends, which do not shrink or grow (Panda et al., 1995).

At high concentrations, MAP2/tau proteins moderately increase the rate of tubulin polymerization and slightly lower its critical concentration (Drechsel et al., 1992), effects that resemble the consequences of subtilisin cleavage of the tubulin COOH termini or increasing the divalent cation concentration. These "charge-shielding" effects enhance polymerization presumably by altering the conformation or charge of the tubulin COOH termini at the growing ends (Wolff et al., 1996). We suggest that the latter effects are distinct from those observed on microtubule dynamics, because they are observed at a different concentration range (Drechsel et al., 1992). The effects on microtubule dynamics were observed with low MAP2 or tau concentrations, whereas effects on the polymerization rate at such concentrations were negligible (Gamblin et al., 1996). Microtubule flexibility also decreased when MAP2c and tau bound to microtubules at low concentrations (Felgner et al., 1997). The convergence of the effects on microtubule dynamics and flexibility at similar concentrations of bound MAPs suggests that both are a result of the MAPs acting on the protofilament conformation.

MTBRs bind tubulin COOH termini and H12, whereas IRs bind H11

We observed the MTBR peaks in the MAP2c difference map to lie along H12. These MTBR peaks contain higher density compared with neighboring regions in the MAP2c difference map and colocalize with the tubulin COOH termini exit sites. Thus, they are likely to be composed of MTBRs and the tubulin COOH termini, both of which presumably become ordered upon binding. This evidence is consistent with NMR data suggesting that MTBR peptides fold when they bind microtubules, interacting with tyrosines within H12 and the tubulin COOH terminus (Kotani et al., 1990). The Au_{11} localization indicates that IRs are bound to the end of H11, suggesting that the sequences of the IRs, not just their lengths (as suggested by Butner and Kirschner, 1991), are crucial for repeat domain function. A combination of recent mutagenesis, peptide, and cross-linking studies has suggested that IR sequences contribute to the microtubule affinity and stabilizing activity of the repeat domain (Goode and Feinstein, 1994; Chau et al., 1998; Goode et al., 2000). Our data are consistent with the idea that IRs and MTBRs bind at adjacent sites and that both are required for stabilizing protofilaments (Fig. 7).

We hypothesize that both IR and MTBR binding to H11 and H12 would influence the conformation of longitudinal tubulin interfaces via the H11-H12 loop. The H11-H12 loop participates in the outer region of the longitudinal tubulin interfaces (Nogales et al., 1999). There are two possible explanations for how the MTBR-IR binding arrangement on tubulins might lead to increased stability at the interfaces. First, MTBR-IR binding to H12 and H11 may possibly influence the flexibility of the intervening loop, in turn affecting the longitudinal interface. Second, the MTBR–COOH terminus complex could act as a physical wedge that stabilizes tubulin interfaces by preventing the straight to curved protofilament conformation. Validation of either possibility must await a high-resolution structure of the MAP2/tau–microtubule complex.

MTBR-IR modules specifically target α or β tubulins

The specific targeting of MAP2c to αβ tubulin dimers is suggested by the localization of Au_{11}–IR-3/4 near only one of the two possible tubulin–tubulin interfaces. As we cannot distinguish α and β tubulin in our 3D maps, we are unable to say whether the IR-3/4 is at the interdimer interface or at the intradimer interface. However, our results suggest that IRs bind to either β–α (interdimer) or α–β (intradimer) regions. Such specific targeting is consistent with the evolutionarily maintained divergence between neighboring IRs and MTBRs (Fig. 1 A). It is notable that many charged residues that lie on the surfaces of H11 and H12 are different in α and β tubulin and this distribution is highly conserved across species (Villasante et al., 1986; Wang et al., 1986; Nogales et al., 1998, 1999). Specificity in targeting requires such differences in the residue distribution on α and β tubulins and in different MTBRs and IRs within the repeat domains.

Comparison with kinesin–microtubule interactions

As suggested here for MAPs, the kinesin motor domain effectively distinguishes between α and β tubulin, because only one motor binds per tubulin heterodimer (Sosa et al., 1997). Specific targeting of α or β tubulin is attained by both kinesin and MAP2c using completely different microtubule binding domains. Furthermore, a class-specific lysine-rich insertion in KIF1A motor domain (termed the K-loop) binds the β tubulin COOH terminus, forming an ordered complex that was observed at medium resolution (Kikkawa et al., 2000), suggesting that the COOH termini induce K-loop folding in the KIF1A. This phenomenon, ordering of the COOH termini and K-loop, is analogous to what we suggest is occurring with the MTBRs in MAP2c. Finally, the overlap between MAP and kinesin binding sites on the protofilament surface suggests that steric interference would occur between these two classes of molecules when both attempt to bind microtubules simultaneously. Such interference probably accounts for the observed effects of MAPs in inhibiting kinesin-based motility, observed in vivo (Ebneth et al., 1998; Trinczek et al., 1999). Thus, the ordered longitudinal binding of MAPs along the outside of the protofilament ridges not only stabilizes microtubules, but also may regulate kinesin-based motility along microtubules.

Materials and methods

Preparation and mutagenesis of recombinant tau and MAP2c

The 467-residue three-repeat rat MAP2c (MAP2c) and the 441-residue four-repeat human tau (tau) cDNAs were inserted in PET3a and PET30 expression vectors as previously described (Lewis et al., 2000; Lim and Halpain, 2000). Proteins were expressed according to previously published methods (Gamblin et al., 1996). MAP2/tau-containing extracts were dialyzed into 50 mM sodium acetate, pH 5.5, 1 mM EDTA, 1 mM EGTA, and 1 mM DTT (dialysis buffer). The dialyzed extracts were loaded onto a HiTrap SP column preequilibrated with 10 vol of dialysis buffer, and washed

with 5 vol of dialysis buffer. Protein was eluted with a continuous (50–700 mM) NaCl gradient. Fractions eluting at 250 mM NaCl were analyzed by SDS-PAGE and then pooled. Each purified full-length protein fraction was dialyzed against 50 mM Tris, pH 7.6, 1 mM EGTA, 1 mM DTT at 4°C, divided into small aliquots, and stored at −80°C.

To generate a cysteine-free mutant of MAP2c, cysteine 348 in MAP2c R3 (Fig. 1 A) was mutated to serine (cf-MAP2c) by site-directed mutagenesis using the primer extension method (Stratagene) with the primer 5′GTTCTTTAGAGAGCCAGATTTGGAAGTC3′ and its complementary strand (Operon). The poorly conserved lysine 364 (Fig. 1 A, asterisk) of MAP2c IR-3/4 was mutated to cysteine in cf-MAP2c (cIR-MAP2c) with the primer 5′TACACTCTCAATGCACACGCGTCCACC3′and its complementary strand (Operon). All point mutagenesis steps were confirmed by DNA sequencing. The cf-MAP2c and cIR-MAP2c mutants were bacterially expressed and purified as described above.

Microtubule binding assays

Microtubules were polymerized by incubating phosphocellulose purified bovine tubulin (Cytoskeleton Co.) at 5 mg/ml in 80 mM Pipes, pH 6.8, 4 mM $MgCl_2$, 1 mM EGTA, 6 mM GTP, 8% DMSO, and 50 μM Taxol for 20 min at 34°C. Polymerized microtubules were then diluted to 0.5 mg/ml into binding buffer (50 mM Pipes, pH 7.6, 1 mM $MgCl_2$, 1 mM EGTA) containing various concentrations of freshly dialyzed MAP2/tau proteins. MAP2/tau proteins with and without microtubules were incubated at 30°C for 1 h to induce microtubule binding, and then spun at 100,000 *g* for 10 min. Supernatants and pellets were separated then analyzed on SDS-PAGE. Molar ratios of tubulin monomer to MAP2/tau proteins were determined by scanning gel bands using a personal densitometer (Molecular Dynamics) equipped with ImageQuant software.

Undecagold cluster labeling

Monomaleimide undecagold clusters were synthesized and attached to Cys 364 of cIR-MAP2c as previously described (Safer et al., 1986; Safer, 1999; Rice et al., 1999). We used a ratio of 10 mol of activated undecagold to 1 mol of cIR-MAP2c to ensure full labeling. The extent of labeling was confirmed by comparing protein concentration determined by SDS-PAGE to undecagold cluster concentration determined by its absorbance at 420 nm (undecagold extinction coefficient $\varepsilon^{\circ} = 470\ M^{-1}cm^{-1}$).

Sample preparation for electron microscopy

Microtubule-saturating MAP2/tau protein concentrations were determined by microtubule binding assays as described above. The MAP2/tau saturated microtubule mixtures (4–5-μl aliquots) were then applied to glow discharged 400-mesh Quantifoil grids with uniform 2-μm hole carbon support films (Signal Probe Co.). After 2 min, the grids were washed with binding buffer containing MAP2/tau protein, which prevents the dissociation of bound MAP2/tau protein, blotted, and frozen by rapidly plunging them into liquid ethane slush (Dubochet et al., 1988). Frozen grids were stored under liquid nitrogen.

Cryo-EM and helical image analysis

A Gatan cryo-stage was used for transfer and observation of frozen grids in a Philips CM200T FEG electron microscope. Electron micrographs were recorded under low-dose conditions (<10 e/Å^2 total dose) at an operating voltage of 120 kV and 40,000 nominal magnification.

Images of 15-protofilament, two-start helical microtubules (assuming tubulin dimer symmetry) were chosen for image analysis (Sosa et al., 1997). Selected micrographs were digitized on a flatbed microdensitometer (PDS 1010G; Perkin-Elmer Corp.) with spot and step sizes equivalent to 4.97 Å at the specimen. The digitized images were analyzed by standard helical reconstruction procedures (DeRosier and Moore, 1970) on Silicon Graphics workstations using the program software package PHOELIX (Whittaker et al., 1995; Carragher et al., 1996). An integral number of microtubule moiré repeats (three to eight) were masked off and Fourier transforms were calculated. Near- and far-side layer lines with Bessel orders up to ±30 and to an axial resolution of 1/18 Å^{-1} were extracted from the transform of each filament. For each of the final 3D maps, datasets were averaged after bringing them to a common phase origin. The moiré repeat and 80-Å and 40-Å layer lines were used for fitting and averaging of the data. An undecorated microtubule dataset was used as a reference for the first phase origin refinement. In the second and third cycles, the average from the previous cycle was used as the new reference. The axial positions of the layer lines were then refined by two cycles of "sniffing" (Morgan and DeRosier, 1992). Final sets of averaged and "sniffed" layer lines were truncated at 1/20 Å^{-1} (Fig. S1) and 3D maps were calculated by Fourier-Bessel inversion and synthesis. The following layer lines (*n*, *l*) were used to calculate the final 3D maps (Fig. S1), where *n* = bessel order and *l* = layer line number: (0, 0); (15, 1); (30, 2); (−17, 17); (−2, 18); (13, 19); (28, 20); (−19, 35); (−4, 36); (11, 37); (26, 38); (−21, 53); (−6, 54); (9, 55); (24, 56).

Difference mapping, statistical analysis, and atomic docking

Each difference map generated was confirmed using statistical difference mapping (Milligan and Flicker, 1987). Individual datasets were moved to a common phase origin and maps were calculated. A mean density and variance were calculated for each voxel in the maps of all datasets, after which a *t* test was used to compare the maps.

Tubulin αβ dimer coordinates (Nogales et al., 1998; Protein Data Bank identification no. 1TUB) were manually docked into the undecorated microtubule 3D map using the program O (Jones et al., 1991) according to the previously published orientation (Nogales et al., 1999). The MAP2 and tau difference maps were displayed at a threshold level corresponding to the expected volume of an MTBR-IR module and the tubulin COOH terminus (31-residue repeat, plus 15-residue tubulin COOH terminus) bound to each tubulin monomer with a specific density of 0.833 D/Å^3. 3D maps were rendered in Volvis (New York State University) and atomic coordinates docked into the 3D maps were rendered in AVS (AVS Corp.)

Online supplemental materials

Fig. S1 shows the layer line data from which MAP2c-decorated, tau-decorated, and undecorated microtubule 3D maps were calculated. Fig. S2 shows 3D maps of MAP2c-decorated, tau-decorated, and undecorated microtubules. Fig. S3 shows the MAP2c, tau, and undecagold statistical difference maps. Online supplemental materials are available at http://www.jcb.org/cgi/content/full/jcb.200201048/DC1.

We thank Drs. Jada Lewis and Michael Hutton (Mayo Clinic, Jacksonville, FL) for the tau construct, and David DeRosier and Nigel Unwin for helpful comments.

J. Al-Bassam is a fellow of the American Heart Association (AHA-0010004Y). R.S. Ozer was supported by a National Institutes of Health fellowship (MH-12504). This work was supported by National Institutes of Health grants GM-52468 (to R.A. Milligan) and MH50861 and AG-05131 (to S. Halpain).

Submitted: 10 January 2002
Revised: 26 April 2002
Accepted: 10 May 2002

References

Aiyar, A. 2000. The use of CLUSTAL W and CLUSTAL X for multiple sequence alignment. *Methods Mol. Biol.* 132:221–241.

Amos, L.A. 1977. Arrangement of high molecular weight–associated proteins on purified mammalian brain microtubules. *J. Cell Biol.* 72:642–654.

Butner, K.A., and M.W. Kirschner. 1991. Tau protein binds to microtubules through a flexible array of distributed weak sites. *J. Cell Biol.* 115:717–730.

Carragher, B.O., M. Whittaker, and R.A. Milligan. 1996. Helical processing using PHOELIX. *J. Struct. Biol.* 116:107–112.

Chau, M.F., M.J. Radeke, C. de Ines, I. Barasoain, L.A. Kohlstaedt, and S.C. Feinstein. 1998. The microtubule-associated protein tau cross-links to two distinct sites on each alpha and beta tubulin monomer via separate domains. *Biochemistry.* 37:17692–17703.

Chen, J., Y. Kanai, N.J. Cowan, and N. Hirokawa. 1992. Projection domains of MAP2 and tau determine spacings between microtubules in dendrites and axons. *Nature.* 360:674–677.

Cleveland, D.W., S.Y. Hwo, and M.W. Kirschner. 1977. Physical and chemical properties of purified tau factor and the role of tau in microtubule assembly. *J. Mol. Biol.* 116:227–247.

Coffey, R.L., and D.L. Purich. 1995. Non-cooperative binding of the MAP-2 microtubule-binding region to microtubules. *J. Biol. Chem.* 270:1035–1040.

Coffey, R.L., J.C. Joly, B.D. Cain, and D.L. Purich. 1994. Exploring the microtubule-binding region of bovine microtubule-associated protein-2 (MAP-2): cDNA sequencing, bacterial expression, and site-directed mutagenesis. *Biochemistry.* 33:13199–13207.

Crowther, R.A., and M. Goedert. 2000. Abnormal tau-containing filaments in neurodegenerative diseases. *J. Struct. Biol.* 130:271–279.

DeRosier, D.J., and P.B. Moore. 1970. Reconstruction of three-dimensional images from electron micrographs of structures with helical symmetry. *J. Mol. Biol.* 52:355–369.

Drechsel, D.N., A.A. Hyman, M.H. Cobb, and M.W. Kirschner. 1992. Modulation of the dynamic instability of tubulin assembly by the microtubule-associated protein tau. *Mol. Biol. Cell.* 3:1141–1154.

Drewes, G., A. Ebneth, U. Preuss, E.M. Mandelkow, and E. Mandelkow. 1997. MARK, a novel family of protein kinases that phosphorylate microtubule-associated proteins and trigger microtubule disruption. *Cell.* 89:297–308.

Drewes, G., A. Ebneth, and E.M. Mandelkow. 1998. MAPs, MARKs and microtubule dynamics. *Trends Biochem. Sci.* 23:307–311.

Dubochet, J., M. Adrian, J.J. Chang, J.C. Homo, J. Lepault, A.W. McDowall, and P. Schultz. 1988. Cryo-electron microscopy of vitrified specimens. *Q. Rev. Biophys.* 21:129–228.

Dye, R.B., S.P. Fink, and R.C. Williams, Jr. 1993. Taxol-induced flexibility of microtubules and its reversal by MAP2 and Tau. *J. Biol. Chem.* 268:6847–6850.

Dyson, H.J., and P.E. Wright. 2002. Coupling of folding and binding for unstructured proteins. *Curr. Opin. Struct. Biol.* 12:54–60.

Ebneth, A., R. Godemann, K. Stamer, S. Illenberger, B. Trinczek, and E. Mandelkow. 1998. Overexpression of tau protein inhibits kinesin-dependent trafficking of vesicles, mitochondria, and endoplasmic reticulum: implications for Alzheimer's disease. *J. Cell Biol.* 143:777–794.

Felgner, H., R. Frank, J. Biernat, E.M. Mandelkow, E. Mandelkow, B. Ludin, A. Matus, and M. Schliwa. 1997. Domains of neuronal microtubule-associated proteins and flexural rigidity of microtubules. *J. Cell Biol.* 138:1067–1075.

Gamblin, T.C., K. Nachmanoff, S. Halpain, and R.C. Williams, Jr. 1996. Recombinant microtubule-associated protein 2c reduces the dynamic instability of individual microtubules. *Biochemistry.* 35:12576–12586.

Garcia, M.L., and D.W. Cleveland. 2001. Going new places using an old MAP: tau, microtubules and human neurodegenerative disease. *Curr. Opin. Cell Biol.* 13:41–48.

Gigant, B., P.A. Curmi, C. Martin-Barbey, E. Charbaut, S. Lachkar, L. Lebeau, S. Siavoshian, A. Sobel, and K. Knossow. 2000. The 4 Å X-ray structure of a tubulin: stathmin-like domain complex. *Cell.* 102:809–816.

Goldstein, L.S., and S. Gunawardena. 2000. Flying through the *Drosophila* cytoskeletal genome. *J. Cell Biol.* 150:F63–F68.

Goode, B.L., and S.C. Feinstein. 1994. Identification of a novel microtubule binding and assembly domain in the developmentally regulated inter-repeat region of tau. *J. Cell Biol.* 124:769–782.

Goode, B.L., M. Chau, P.E. Denis, and S.C. Feinstein. 2000. Structural and functional differences between 3-repeat and 4-repeat tau isoforms. Implications for normal tau function and the onset of neurodegenetative disease. *J. Biol. Chem.* 275:38182–38189.

Gustke, N., B. Trinczek, J. Biernat, E.M. Mandelkow, and E. Mandelkow. 1994. Domains of tau protein and interactions with microtubules. *Biochemistry.* 33:9511–9522.

Himmler, A., D. Drechsel, M.W. Kirschner, and D.W. Martin, Jr. 1989. Tau consists of a set of proteins with repeated C-terminal microtubule-binding domains and variable N-terminal domains. *Mol. Cell. Biol.* 9:1381–1388.

Hirokawa, N. 1982. Cross-linker system between neurofilaments, microtubules, and membranous organelles in frog axons revealed by the quick-freeze, deep-etching method. *J. Cell Biol.* 94:129–142.

Ichihara, K., H. Kitazawa, Y. Iguchi, H. Hotani, and T.J. Itoh. 2001. Visualization of the stop of microtubule depolymerization that occurs at the high-density region of microtubule-associated protein 2 (MAP2). *J. Mol. Biol.* 312:107–118.

Joly, J.C., G. Flyn, and D.L. Purich. 1989. The microtubule-binding fragment of microtubule-associated protein-2: location of the protease-accessible site and identification of an assembly-promoting peptide. *J. Cell Biol.* 109:2289–2294.

Jones, T.A., J.Y. Zou, S.W. Cowan, and M. Kjeldgaard. 1991. Improved methods for building protein models in electron density maps and the location of errors in these models. *Acta Crystallogr A.* 47:110–119.

Kikkawa, M., Y. Okada, and N. Hirokawa. 2000. 15 A resolution model of the monomeric kinesin motor, KIF1A. *Cell.* 100:241–252.

Kotani, S., G. Kawai, S. Yokoyama, and H. Murofushi. 1990. Interaction mechanism between microtubule-associated proteins and microtubules. A proton nuclear magnetic resonance analysis on the binding of synthetic peptide to tubulin. *Biochemistry.* 29:10049–10054.

Kowalski, R.J., and R.C. Williams, Jr. 1993. Microtubule-associated protein 2 alters the dynamic properties of microtubule assembly and disassembly. *J. Biol. Chem.* 268:9847–9855.

Leclerc, N., P.W. Baas, C.C. Garner, and K.S. Kosik. 1996. Juvenile and mature MAP2 isoforms induce distinct patterns of process outgrowth. *Mol. Biol. Cell.* 7:443–455.

Lee, G., R.L. Neve, and K.S. Kosik. 1989. The microtubule binding domain of tau protein. *Neuron.* 2:1615–1624.

Lewis, J., E. McGowan, J. Rockwood, H. Melrose, P. Nacharaju, M. Van Slegtenhorst, K. Gwinn-Hardy, M. Paul Murphy, M. Baker, X. Yu, et al. 2000. Neurofibrillary tangles, amyotrophy and progressive motor disturbance in mice expressing mutant (P301L) tau protein. *Nat. Genet.* 25:402–405.

Lewis, S.A., D.H. Wang, and N.J. Cowan. 1988. Microtubule-associated protein MAP2 shares a microtubule binding motif with tau protein. *Science.* 242: 936–939.

Lim, R.W., and S. Halpain. 2000. Regulated association of microtubule-associated protein 2 (MAP2) with Src and Grb2: evidence for MAP2 as a scaffolding protein. *J. Biol. Chem.* 275:20578–20587.

Ludin, B., K. Ashbridge, U. Funfschilling, and A. Matus. 1996. Functional analysis of the MAP2 repeat domain. *J. Cell Sci.* 109:91–99.

Mandelkow, E.M., E. Mandelkow, and R.A. Milligan. 1991. Microtubule dynamics and microtubule caps: a time-resolved cryo-electron microscopy study. *J. Cell Biol.* 114:977–991.

Mickey, B., and J. Howard. 1995. Rigidity of microtubules is increased by stabilizing agents. *J. Cell Biol.* 130:909–917.

Milligan, R.A., and P.F. Flicker. 1987. Structural relationships of actin, myosin, and tropomyosin revealed by cryo-electron microscopy. *J. Cell Biol.* 105:29–39.

Milligan, R.A., M. Whittaker, and D. Safer. 1990. Molecular structure of F-actin and location of surface binding sites. *Nature.* 348:217–221.

Mitchison, T., and M.W. Kirschner. 1984. Dynamic instability of microtubule growth. *Nature.* 312:237–242.

Morgan, D.G., and D. DeRosier. 1992. Processing images of helical structures: a new twist. *Ultramicroscopy.* 46:263–285.

Muller-Reichert, T., D. Chretien, F. Severin, and A.A. Hyman. 1998. Structural changes at microtubule ends accompanying GTP hydrolysis: information from a slowly hydrolyzable analogue of GTP, guanylyl (alpha,beta) methylenediphosphonate. *Proc. Natl. Acad. Sci. USA.* 95:3661–3666.

Nogales, E., S.G. Wolf, and K.H. Downing. 1998. Structure of the alpha beta tubulin dimer by electron crystallography. *Nature.* 391:199–203.

Nogales, E., M. Whittaker, R.A. Milligan, and K.H. Downing. 1999. High-resolution model of the microtubule. *Cell.* 96:79–88.

Ozer, R.S., and S. Halpain. 2000. Phosphorylation-dependent localization of microtubule-associated protein MAP2c to the actin cytoskeleton. *Mol. Biol. Cell.* 11:3573–3587.

Panda, D., B.L. Goode, S.C. Feinstein, and L. Wilson. 1995. Kinetic stabilization of microtubule dynamics at steady state by tau and microtubule-binding domains of tau. *Biochemistry.* 34:11117–11127.

Paschal, B.M., R.A. Obar, and R.B. Vallee. 1989. Interaction of brain cytoplasmic dynein and MAP2 with a common sequence at the C terminus of tubulin. *Nature.* 342:569–572.

Rice, S., A.W. Lin, D. Safer, C.L. Hart, N. Naber, B.O. Carragher, S.M. Cain, E. Pechatnikova, E.M. Wilson-Kubalek, M. Whittake, et al. 1999. A structural change in the kinesin motor protein that drives motility. *Nature.* 402:778–784.

Safer, D. 1999. Undecagold cluster labeling of proteins at reactive cysteine residues. *J. Struct. Biol.* 127:101–105.

Safer, D., L. Bolinger, and J.S. Leigh, Jr. 1986. Undecagold clusters for site-specific labeling of biological macromolecules: simplified preparation and model applications. *J. Inorg. Biochem.* 26:77–91.

Schweers, O., E. Schonbrunn-Hanebeck, A. Marx, and E. Mandelkow. 1994. Structural studies of tau protein and Alzheimer paired helical filaments show no evidence for beta-structure. *J. Biol. Chem.* 269:24290–24297.

Serrano, L., J. Avila, and R.B. Maccioni. 1984. Controlled proteolysis of tubulin by subtilisin: localization of the site for MAP2 interaction. *Biochemistry.* 23: 4675–4681.

Serrano, L., E. Montejo de Garcini, M.A. Hernandez, and J. Avila. 1985. Localization of the tubulin binding site for tau protein. *Eur. J. Biochem.* 153:595–600.

Sosa, H., D.P. Dias, A. Hoenger, M. Whittaker, E. Wilson-Kubalek, E. Sablin, R.J. Fletterick, R.D. Vale, and R.A. Milligan. 1997. A model for the microtubule-Ncd motor protein complex obtained by cryo-electron microscopy and image analysis. *Cell.* 90:217–224.

Spero, D.A., and F.J. Roisen. 1985. Neuro-2a neuroblastoma cells form neurites in the presence of taxol and cytochalasin. *Brain. Res.* 355:155–159.

Trinczek, B., A. Ebneth, E.M. Mandelkow, and E. Mandelkow. 1999. Tau regulates the attachment/detachment but not the speed of motors in microtu-

bule-dependent transport of single vesicles and organelles. *J. Cell Sci.* 112: 2355–2367.

Villasante, A., D. Wang, P. Dobner, P. Dolph, S.A. Lewis, and N.J. Cowan. 1986. Six mouse alpha-tubulin mRNAs encode five distinct isotypes: testis-specific expression of two sister genes. *Mol. Cell. Biol.* 6:2409–2419.

Voter, W.A., and H.P. Erickson. 1982. Electron microscopy of MAP 2 (microtubule-associated protein 2). *J. Ultrastruct. Res.* 80:374–382.

Wang, D., A. Villasante, S.A. Lewis, and N.J. Cowan. 1986. The mammalian beta-tubulin repertoire: hematopoietic expression of a novel, heterologous beta-tubulin isotype. *J. Cell Biol.* 103:1903–1910.

Whittaker, M., B.O. Carragher, and R.A. Milligan. 1995. PHOELIX: a package for semi-automated helical reconstruction. *Ultramicroscopy.* 58:245–259.

Williamson, J.R. 2000. Induced fit in RNA-protein recognition. *Nat. Struct. Biol.* 7:834–837.

Wolff, J., L. Knipling, and D.L. Sackett. 1996. Charge shielding and the "paradoxical" stimulation of tubulin polymerization by guanidine hydrochloride. *Biochemistry.* 35:5910–5920.